1990A&A...237..409P

Astron. Astrophys. 237, 409–424 (1990)

ASTRONOMY AND ASTROPHYSICS

Radiation-driven winds of hot luminous stars

VIII. The bistable wind of the luminous blue variable P Cygni (B1 Ia$^+$)

A.W.A. Pauldrach and J. Puls

Institut für Astronomie und Astrophysik der Universität München, Scheinerstr. 1, D-8000 München 80, Federal Republic of Germany

Received March 31, 1989; accepted March 9, 1990

Abstract. In order to explain the peculiar observed characteristics of the wind of P Cygni – rather high mass loss rate, extremely low terminal velocity, very slow acceleration to terminal velocity, variability of the wind – a grid of wind models is calculated representing the range of likely stellar parameters and evolutionary phases of the star. The models have been constructed using our recently improved radiation-driven wind code. The results show that the self-consistent hydrodynamical wind solution of our final model reproduces the observed mass loss rate and terminal velocity, and that the observed IR excess is almost perfectly fitted by the derived velocity structure. The comparison between the observed and calculated wind dynamics places constraints on the stellar parameters, narrowing the uncertainty on their values more than had hitherto been possible. The stellar parameters which are compatible with the wind properties are, with a high degree of confidence: $\log L/L_\odot = 5.86$, $\log g = 2.04$, $R_* = 76\,R_\odot$, yielding a mass of $23\,M_\odot$ and therefore setting a constraint on the evolutionary stage of the star. Our self-consistent non-LTE calculations of the model grid further reveal a bi-stability of the wind of P Cygni. We demonstrate that P Cygni's wind is highly unstable with respect to extremely small changes in radius $\Delta R/R > 1.5\%$ or luminosity $\Delta L/L > 3\%$. Moreover, on the basis of the bi-stability we discuss a "feed-back" mechanism, which might explain the variability of P Cygni's wind.

Key words: luminous blue variables – non-LTE – mass loss – winds

1. Introduction

In recent years the study of luminous blue variables (LBVs) has played an important role in furthering our understanding of the evolution of extremely massive stars. All LBVs are located close to the Humphreys-Davidson limit at the top of the HR-diagram, which supports strongly Maeder's suggestion (see Maeder, 1983; Maeder and Meynet, 1987, hereafter MM) that stars with initial masses greater than about 40 to $50\,M_\odot$ do not evolve into red supergiants but turn into Wolf-Rayet stars after their LBV phase. Also they are unstable, being characterized by high mass loss rates – typically ten times higher than those found for normal supergiants (see Lamers, 1987) – episodes of shell ejection and large eruptions, which must strongly influence the evolution of LBVs from (presumably) O and Of stars.

The significance of the LBVs is therefore obvious, but a breakthrough in this subject is hampered by our ignorance of the mechanisms that produce the high mass loss rates, the shell ejection and the outbursts, as well as by the problem of establishing exactly both the location of the stars on the HR diagram and their evolutionary phase.

In order to assess the situation specifically we concentrate on a subgroup of the LBVs, the "P Cygni Type" variables (PCT, for a definition see Lamers, 1986a), and the most famous star within this group, P Cygni itself, is discussed in its quiescent phase. A phase of quiescence means in practice that the occurrence of phases of major activity, like outbursts, is not discussed. This is not a bad approximation, since the last major active phase, where outbursts were observed occurred in the seventeenth century and is the only one known (see the review by Lamers, 1986a). Nevertheless, P Cygni shows irregular variations in the visual and UV line profiles even in this quiet phase. These variations are explained by the non-periodic ejection of shells, which occurs on a time scale of about 60 to 100 days (see van Gent and Lamers, 1986).

The features of the 'quiescent' wind of P Cygni are also peculiar, since they are considerably different from those of winds of normal supergiants: the mass loss rate of P Cygni is higher by a factor five, the terminal velocity is smaller by a factor ten and the velocity law itself is much flatter (see Lamers, 1986; Waters and Wesselius, 1986). Although Lamers (1986) has estimated that the radiative force of weak lines may be responsible for the slow acceleration and Pauldrach, Puls and Kudritzki (1986) have reproduced the high mass loss rate and the low terminal velocity in the context of the theory of radiation driven winds in a "quasi" – self-consistent treatment (see below), the slow velocity law has caused uncertainty on whether PCT winds are driven entirely by radiation pressure. However, despite the uncertainty concerning the present evolutionary phase of P Cygni, the star is obviously evolving from the main-sequence up to the luminosity limit and has thus already lost a considerable fraction of its mass. This means that the star is not very far from the Eddington limit, and this of course influences the 'quiescent' wind features such that they may differ drastically from those of normal supergiant's winds. Hence, it is worthwhile to investigate whether the observed characteristics of P Cygni's wind can be explained by means of our recently improved self-consistent non-LTE treatment of radiation driven winds (see Pauldrach et al., 1986 (Paper I); Pauldrach, 1987 (Paper III); Puls, 1987 (Paper IV); Pauldrach and

Send offprint requests to: A.W.A. Pauldrach

© European Southern Observatory • Provided by the NASA Astrophysics Data System

1990A&A...237..409P

Herrero, 1988). However, this requires calculations which are performed over a large model grid, because for one thing the evolutionary stage of P Cygni is uncertain, and, secondly, for objects close to the Eddington limit, the wind properties depend strongly on the stellar parameters and especially on the ratio L/M (see also Pauldrach et al., 1989). However, the present determination of these parameters is not accurate enough to constrain the parameter space for practical calculations. This is discussed in Sect. 2, where we also discuss whether the linear velocity law adopted by Waters and Wesselius (1986) for the fit of the observed IR fluxes is really the only one which reproduces the IR flux and the IR excess (see also Puls et al., 1989). The dynamical results of the grid of wind models we chose is presented in Sect. 3. We also discuss in that section whether a comparison of the results from the model grid with the observed dynamical parameters ($\dot{M}$, v_∞) of the wind of P Cygni can set constraints on the adopted stellar parameters in the sense that the uncertainties on their value and therefore on the current evolutionary phase of the star can be reduced. Furthermore, the choice of our model grid allows us to investigate whether P Cygni's wind is stable against small changes in the stellar parameters. This is also done in Sect. 3, where our detection of a bistability (see also Pauldrach et al., 1989a) of the wind of P Cygni is discussed by means of a self-triggering mechanism, which might explain the observed irregular shell ejections episodes. In Sect. 4 we present our final, most elaborate model and demonstrate that not only the mass loss rate and the terminal velocity, but also the observed IR excess is reproduced by our *self-consistent hydrodynamical wind solution.* Finally, Sect. 5 gives a summary and conclusions.

2. The basic parameters of P Cygni and the model grid

Since our treatment of the theory of radiation driven winds is in its present stage in principle self-consistent (see below), only the three physical stellar parameters need to be specified for our calculations. These free parameters are the photospheric radius, R_*, which is defined by a certain optical depth (e.g. $\tau_R = 1$), the effective temperature, $T_{\rm eff}(R_*)$, and the gravity, $\log g(R_*)$, or the mass M_*. All these quantities need to be determined accurately because the calculated wind dynamics, as was already mentioned in previous papers (see for instance Pauldrach, 1987), depend crucially on these free parameters. This is particularly true for objects close to the Eddington-limit (see Pauldrach et al., 1989, Paper VII).

Although detailed investigations have been carried out for P Cygni, only estimates of the basic parameters ($T_{\rm eff}$, R_*) are available due to the poor knowledge of the interstellar extinction in the direction of P Cygni and to the related uncertainty of the energy distribution (see Lamers et al., 1983). Since the third quantity, the mass, can be derived only from evolutionary tracks, the situation is in this case particularly awkward because of uncertainties in the evolutionary phase and in the luminosity of P Cygni.

In view of these problems, we performed our calculations over a large model grid of stellar parameters. As a basis of this grid we used the sets of values $T_{\rm eff} = 19\,300$ K, $\log L/L_\odot = 5.97, 5.86, 5.74$ and $T_{\rm eff} = 18\,300$ K, $\log L/L_\odot = 5.6, 5.7, 5.8$, which were derived by Lamers et al. (1983) for $E(B-V) = 0.63$ and $E(B-V) = 0.58$, respectively (see also Lamers et al., 1983, Table 5). The masses have been derived according to the effective temperatures, from the evolutionary tracks recently obtained by Maeder and Meynet (1987 – MM), which include mass-loss and overshooting. Since the evolutionary phase of P Cygni is unknown, we have adopted the $M-L$ relation for TAMS as well as that for post-RGB objects, where the latter assumption represents the hypothesis that the star is presently evolving into a Wolf-Rayet star. Moreover, we have accounted for the uncertainty in the mass due to the evolutionary calculations by simply adopting different masses for constant luminosities and fixed temperatures. This is reasonable, not only because of the large uncertainties in the determination of the mass for objects in the RGB phase, but also in view of the possibility that P Cygni may have evolved directly from the main sequence (see Wolf et al., 1981), which would of course yield a different $M-L$ relationship. The parameters for our sets of model grid points ($T_{\rm eff} = 19\,300$ K, $18\,300$ K) are shown in Table 1 and a graphical presentation is given in Fig. 1 (only the first set is shown, because the results for the second one are not as remarkable), and they will be discussed briefly in the next section.

The computer code used to perform our calculations has its origins in codes that treat the hydrodynamics (Paper I), the ionization coupled with radiation transfer (Paper III; Pauldrach and Herrero, 1988) and the multi-line transfer problem (Paper IV). Since the whole procedure was recently described by Pauldrach et al. (1989) and the revision which the coding has undergone in order to adapt it to the conditions of P Cygni was not extensive, we only repeat briefly the most important points.

Based on calculations of the detailed statistical equilibrium for 26 elements in their different ionization stages together with continuum and line radiation transfer, line forces are obtained, and parameterized for the hydrodynamic calculations using the force multiplier concept. In doing so the force multiplier parameter triplet (k, α, δ) is not held fixed, as was originally proposed by Abbott (1982), but is allowed to change with depth in the wind. This approach turned out to be crucial in order to reach convergence for P Cygni. Using these depth dependent line forces the hydrodynamic structure is computed using the finite cone angle effect. Since the force multiplier parameters and the continuum force, which we restricted to Thomson scattering depend on the dynamical structure and on the degree of ionisation, an iteration cycle is necessary. An iteration is also necessary for the inclusion of multi-line effects.

In addition to the stellar parameters the code depends also

i) on elemental abundances (solar composition has been used for the present calculations);

ii) on the emergent fluxes of plane-parallel photospheric models (Kurucz, 1979), which are used in the optically thin part of the wind ($\tau_\nu < 1$) as an inner radiative boundary condition; (in the optically thick part of the wind ($\tau_\nu > 1$, in the case of P Cygni shortwards of the H I groundstate edge) $I_\nu^+ = S_\nu\,(1 - 1/2 e^{-3^{1/2}\tau_\nu})$ is used as an inner boundary condition, where S_ν is expressed in terms of the corresponding departure coefficients; it should be noted that in order to avoid instabilities the departure coefficients are only updated after a couple of iterations).

iii) on the temperature structure in the wind, which was set to be either constant and equal to the effective temperature, throughout the wind, or, for the sake of comparison, equal to the temperature structure derived by Drew (1985) for P Cygni.

In order to check our theoretical predictions concerning the wind structure, observational data for the terminal velocity, mass loss rate and velocity structure are additionally required. Surprisingly, in contrast to normal luminous stars, the value of the

© European Southern Observatory • Provided by the NASA Astrophysics Data System

1990A&A...237..409P

Table 1. Stellar parameters of the model grid

$T_{\rm eff}$ (10^3 K)	$R/R_\odot$	$\log(L/L_\odot)$	$M/M_\odot$	$\log(g)$ (cgs)	$\Gamma_{\rm s.p.}$	$v_{\rm esc}$ (km s^{-1})	Model
Post-RGB							
			24.5	2.185	0.535	257	1
			* 19.5	2.080	0.680	193	2
			18.8	2.070	0.698	181	2a
	66	5.74	18.3	2.060	0.700	177	2b
			17.5	2.040	0.734	164	2c
			16.5	2.016	0.784	143	3
			15.5	1.990	0.839	120	3a
			15.0	1.975	0.862	110	4
			14.5	1.960	0.892	95	5
			28.5	2.130	0.607	239	1
			* 23.5	2.050	0.725	180	2
			22.5	2.030	0.774	159	2a
19.3	76	5.86	20.5	1.990	0.832	132	3
			19.0	1.955	0.897	99	4
			18.5	1.940	0.921	85	5
			34.0	2.100	0.650	230	1
			* 29.0	2.030	0.760	175	2
	86	5.97	27.5	2.010	0.800	156	2a
			26.0	1.990	0.845	135	3
			24.5	1.958	0.896	106	4
			24.0	1.940	0.915	94	5
			* 16.0	2.060	0.586	204	
	62	5.6	14.0	1.999	0.670	170	
			12.5	1.950	0.765	140	
18.3	70	5.7	* 18.8	2.020	0.627	194	
			16.8	1.970	0.700	162	
	78	5.8	* 21.6	1.988	0.688	183	
TAMS							
	66	5.74	* 34.0	2.330	0.400	384	
19.3	76	5.86	* 38.1	2.260	0.450	326	
	86	5.97	* 41.5	2.190	0.570	296	

* Exact $M-L$ relation according to Maeder and Meynet (1987)

terminal wind velocity for P Cygni is uncertain. Cassatella et al. (1979) found from the Mg II and Fe II lines a value of 300 km s^{-1}, whereas Lamers et al. (1985) argued that the blue absorption edges are contaminated by turbulent motion, and that the true terminal velocity is 206 km s^{-1}.

The usual way to determine mass loss rates is the use of radio observations, assuming the radiation to be produced entirely by thermal ff- and bf-processes. In view of the evolutionary scenario of P-Cygni, several authors (Lamers et al., 1983a; Waters et al., 1986) proposed that part of this emission could be produced by cold dust from the remnant of a suspected old red supergiant wind ($v_\infty = 10-20$ km s^{-1} at about 15000 R_*). It is therefore worthwhile to investigate P-Cygni's radio emission in more detail, especially since all previous mass loss determinations were performed – to the authors' knowledge – using only one frequency point. Fortunately P-Cygni is extremely well observed at different wavelengths ranging from 0.33 to 20 cm. Figure 2a shows the compilation by Wendker (1987) indicating also three phases of extended emission (*, cf. Sect. 3) and two observations where the object was resolved (◇, observation at 6 cm by White and Becker

© European Southern Observatory • Provided by the NASA Astrophysics Data System

1990A&A...237..409P

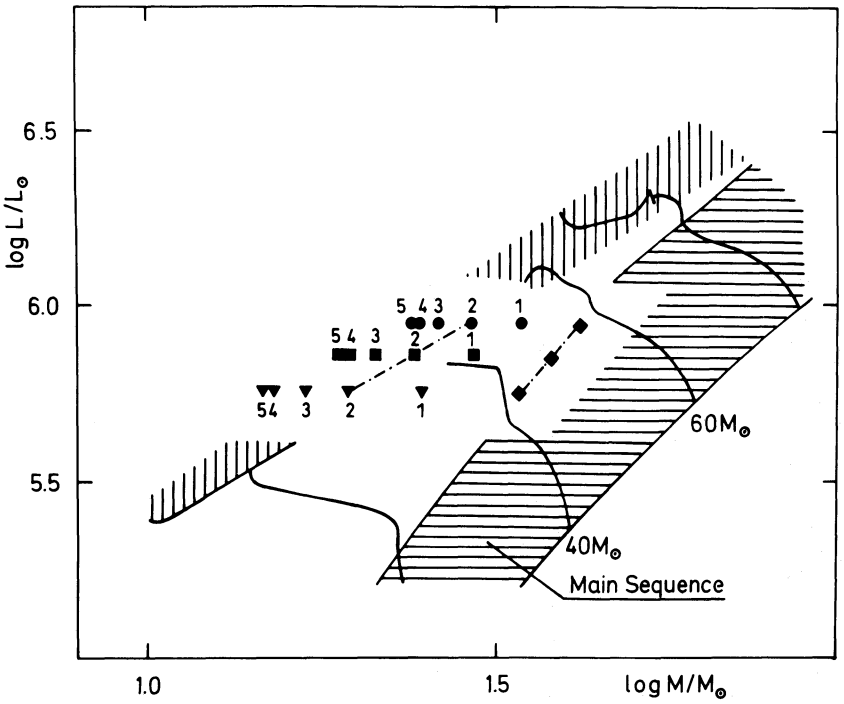

Fig. 1. The mass-luminosity diagram for the model grid. The models 2●, 2■, 2▼, are calculated for $\log(L/L_\odot)=5.97, 5.86, 5.74$ (Lamers et al., 1983) and the respective masses predicted by evolutionary tracks from Maeder and Meynet (1987) for $T_{\rm eff}=19\,300$ K. Thus the dashed line on the left is the $M-L$ relation for post RGB objects and the one on the right (connected to ◆) is the $M-L$ relation for TAMS at the temperature of P Cygni. The other sequences of models (1, 3, 4, 5) yield the stellar parameters, if we distrust the accuracy of the evolutionary calculations due to the large uncertainties in the value of M in the RGB phase and adopt different masses at $T_{\rm eff}=19\,300$ K for constant luminosities

(1982), observation at 2 cm by Becker and White, 1985). For a purely thermal emission model, the observed flux should follow a power law (cf. Wright and Barlow, 1975; Panagia and Felli, 1975; Lamers and Waters, 1984; Waters and Lamers, 1984).

$$F_\nu \sim (\dot{M}/v_\infty)^{4/3} 1/d^2\, \lambda^{-0.6},$$

where the ff-gaunt factor from Allen (1973) was used. Although a maximum likelihood analyses of the plotted data yields a spectral power index of -0.762 (standard deviation $\pm 10\%$ in the log) a subsequent χ^2 test does not exclude the thermal index of -0.6, but reveals (with a slightly larger standard deviation of $\pm 12\%$) even a larger significance level in this case. We conclude therefore, that the measured radio flux is predominantly of thermal nature and can be actually used for direct mass loss determination. With an electron temperature of $T_e \approx 20\,000$ K, a distance of $d=1.8 \pm 0.1$ kpc (Lamers et al., 1983) we finally derive

$$\dot{M}(10^{-6} M_\odot\,{\rm yr}^{-1})/v_\infty({\rm km\,s}^{-1}) = 4.177\ (+1.45/-1.07)\,10^{-2}.$$

For the two values of the terminal velocities considered this gives a mass loss rate of 8.6 $(+2.7/-2.4)\,10^{-6} M_\odot\,{\rm yr}^{-1}$ for $v_\infty = 206\,{\rm km\,s}^{-1}$ or 12.5 $(+4.3/-3.2)\,10^{-6} M_\odot\,{\rm yr}^{-1}$ for $v_\infty = 300\,{\rm km\,s}^{-1}$.

A more difficult problem is the determination of the velocity law. Using the ground-based IR fluxes by Abbott et al. (1984, 0.98–20 μm) and the IRAS fluxes (10–100 μm), Waters et al. (1986) argued that the best fit could be obtained with a *linear* velocity law $v(r)=v_\infty\,(0.1+0.057(r/R_*-1))$, where the fluxes at 60 and 100 cm are due to enhanced emission by dust or originate from a shell at $r \approx 15\,R_*$. *This fit, however, is not unique.* A typical β-velocity law – which was excluded by Waters et al. (1986) – with $\beta=4$ (firstly proposed by Barlow and Cohen (1977)) and a much smaller initial velocity ($v_0 = 4\,10^{-4} v_\infty$), for the same stellar and wind parameters as given by Waters et al., reproduces the observed IR flux (Fig. 2b) and the IR-excess (not shown) just as well (see also Castor and Lamers, 1979). The reason for this behaviour is that both the linear and the $\beta=4$ velocity law yield the same density structure in the IR-emitting region (Fig. 2c).

An additional strong argument supporting our assumption of a β-velocity law is given by the wind acceleration mechanism: Lamers (1986), on the basis of a linear velocity law, showed that turbulent pressure, dissipating sound waves and pure continuum pressure are all unable to provide sufficient acceleration to drive P Cygni's wind. He concluded that the acceleration must be due to radiation pressure, probably on a large number of *optically thin* lines in the Balmer continuum. Simple algebra, however, shows that the radiative acceleration necessary to *yield* the *linear* velocity law can only arise if the optically thin lines are effective in driving the wind only in its lower part ($r<3R_*$, $v<0.22v_\infty$), whereas in the outer part the wind must be accelerated only by optically thick lines (see Appendix). In order to test this constraint, we ran the NLTE-code for the parameters of P Cygni and calculated the line force resulting from the linear velocity field. It turned out that the linear velocity law gives rise to an acceleration from both optically thick (60%) and optically thin lines (40%), *throughout the wind.* This contradicts strongly the assumptions and shows that a linear velocity law cannot be obtained by radiative acceleration for an object like P Cygni. For the β-velocity law, however, the situation looks much better. The NLTE line force (including line overlap) resulting from the calculations turns out to be nearly identical to that necessary for building up the β-law. Hence, it is most likely that the acceleration mechanism driving the wind in the case of P Cygni wind is line pressure, resulting in a velocity field which has the typical β-structure of radiatively driven winds and which should give rise to the observed IR excess. This intermediate result will be checked in the following sections by means of our self-consistent calculations.

In this context it is also important to investigate the validity of the *S*obolev *a*pproximation (SA), which is applied for calculating

© European Southern Observatory • Provided by the NASA Astrophysics Data System

1990A&A...237..409P

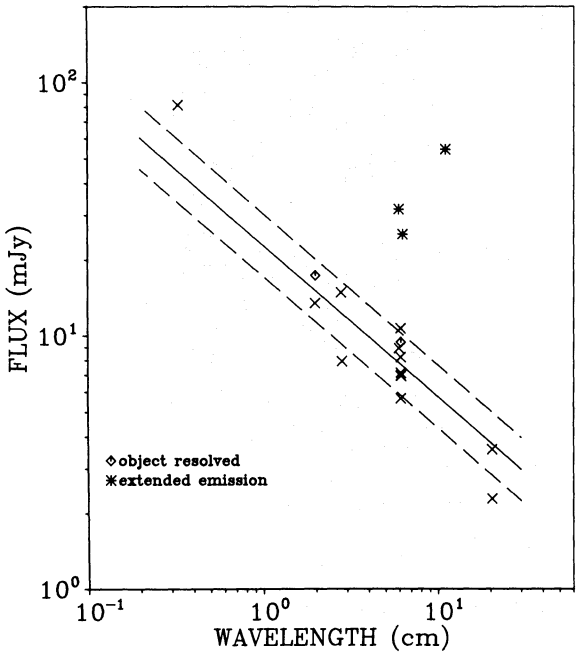

Fig. 2a. Radio observations of P-Cygni (0.33–20 cm) from the compilation by Wendker (1979). The bold line gives the best fit to the data assuming $d \log F_\nu / d \log \lambda = -0.6$ (thermal emission model), the dashed lines represent the standard deviation. Also indicated: ✳ extended emission, 〈 〉 object resolved (references see text)

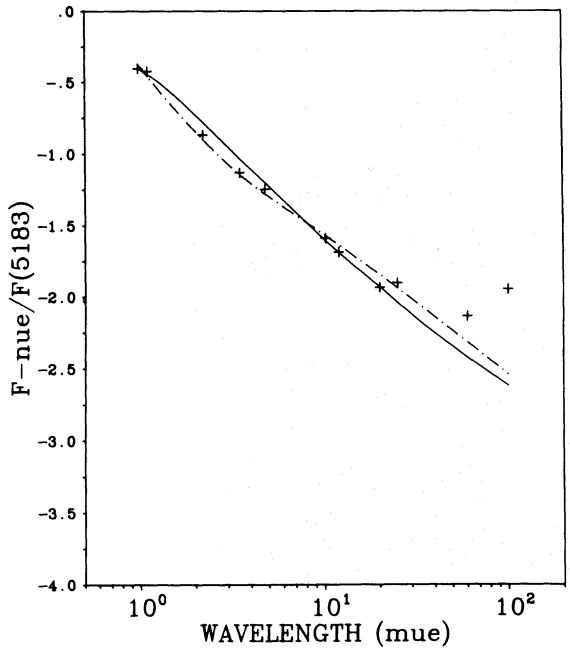

Fig. 2b. Comparison of calculated IR-fluxes ($F_\nu / F_{5183\text{Å}}$) to observations: Model parameters from Waters et al. (1986), observations (+) by Abbott et al. (1984, 0.98–10 μm) and Waters et al. (1986, IRAS, 10–100 μm). Dashed-dotted: linear velocity law; bold: $\beta = 4$ velocity law

line forces and escape probabilities in our code. Lamers (1986) has argued that the SA is not valid in the case of P-Cygni because of the small (constant) value of the velocity gradient. With this argument, the difference between the "observed" and the theoretically predicted line acceleration should be explained. However, the "observed" value of the acceleration was *calculated from the linear velocity law* and the theoretical value by extrapolating Abbott's (1982) grid of force-multipliers with its approximative treatment of ionization balance (based on the assumption that all lines are optically thick and that the complete ionizing continuum is optically thin throughout the wind (cf. Paper III)).

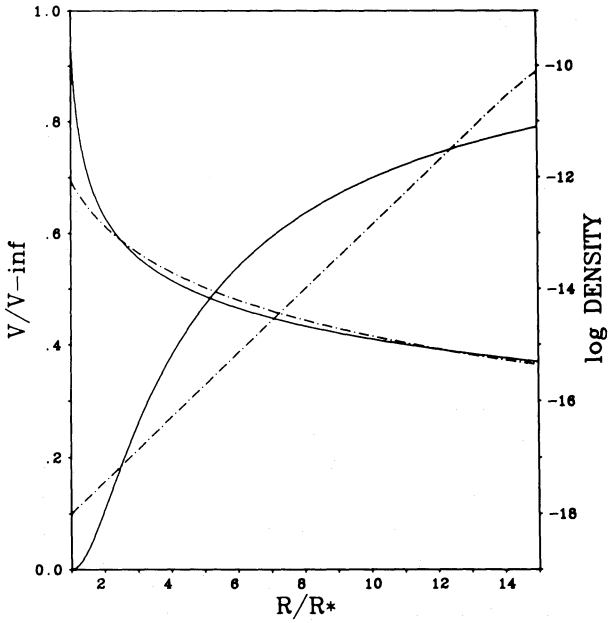

Fig. 2c. Comparison of velocity and density structure for the linear (dashed-dotted) and $\beta = 4$ (fully drawn) velocity law

Applying the $\beta = 4$ velocity law, one finds for most lines the SA to be valid, i.e.

$$dv/dr \gg v_D/r$$

from $r >= 1.3\, R_*$, depending on the atomic weight of the considered ion. Even with a Doppler velocity $v_D = 10\,\mathrm{km\,s^{-1}}$, as used by Lamers, the approximation holds from $r >= 1.5\, R_*$. This result was independently checked by calculating the complete radiative transfer (g^L_{rad}, $\bar{J}_L$, $\bar{H}_L$ for all lines) with our comoving frame code. As was already shown in Paper I (cf. also Puls and Hummer, 1987), the SA turned out to be valid even below the sonic point, both in the escape probabilities and in the line force. The latter is shown in Fig. 13, where the difference between exact quantity and SA approximation is negligible in the lower part of the wind. The difference in the outer part is caused mainly by line blocking and is independent of the applied radiative transfer, if the multi-line effects are included (see Paper IV). Only in the innermost part of the wind the exactly calculated line force is considerably larger (by a factor 10 to 100). However, here the absolute value of the force is small compared to the dominating Thomson force. Therefore, we conclude that applying the SA for the wind of P Cygni leads to no significant errors, neither in the total acceleration nor in the escape probabilities.

3. Dynamical properties for models at different evolutionary stages

The atmospheric characteristics of PCT stars differ drastically from those of normal early-type stars, since PCT's are not

© European Southern Observatory • Provided by the NASA Astrophysics Data System

1990A&A...237..409P

Table 2. Computed mass-loss rates and terminal velocities for models corresponding to the $M-L$ relation for TAMS

$T_{\rm eff}$ (10^3 K)	$\log(L/L_\odot)$	$M/M_\odot$	$\dot{M}$ ($10^{-6} M_\odot\,{\rm yr}^{-1}$)	v_∞ (km s^{-1})	$v_\infty/v_{\rm esc}$	$\dot{M}/v_\infty$ ($10^{-8} M_\odot\,{\rm yr}^{-1}$) (km s^{-1})
	5.74	34.0	1.0	800	2.1	0.13
19.3	5.86	38.1	1.4	740	2.3	0.19
	5.97	41.5	2.5	564	1.9	0.44

expected to be approaching the RGB. For the range of luminosity of P Cygni, for example, we would expect a normal supergiant mass loss rate of about $3\,10^{-6} M_\odot\,{\rm yr}^{-1}$ (see for instance Paper VII; or Howarth and Prinja, 1989), a value which is about 5 times smaller than the observed one. Although no exact calculations have been performed that confirm this, we feel that the possibility that P Cygni is on its way to the RGB can be excluded.

The results of the calculations (marked by diamonds in Fig. 1) with respect to v_∞ and $\dot{M}$ are summarized in Table 2. It can be clearly seen that v_∞ is 2 to 3 times larger than observed and that $\dot{M}$ is in fact smaller by a factor five to ten. Hence, we can conclude from these calculations that P Cygni's mass does indeed not correspond to the $M-L$ relation for TAMS. In the following we will then concentrate on models for evolutionary phases leading to ratios of stellar to Eddington-luminosity $\Gamma = L/L_{\rm E}$ closer to unity, which is different from the values typical for normal supergiants.

The theory of radiation-driven winds predicts for such objects a strong dependence of the mass loss rate not only on the line acceleration, resulting from the line force calculated accounting for the NLTE occupation numbers of 133 ions, but also on Γ, as follows:

$$\dot{M} = (kL)^{1/(\alpha-\delta)} \left(\frac{1}{M(1-\Gamma)}\right)^{(1-\alpha)/(\alpha-\delta)} \tag{1}$$

(see Paper I), where Γ is expressed in terms of the Thomson scattering cross-section, $\sigma_{\rm Th}$, the local electron density, $n_{\rm e}(r)$, the particle density, $\rho(r)$, the stellar mass and luminosity, as follows:

$$\Gamma(r) = 7.56\,10^{-5}\,\sigma_{\rm Th}[n_{\rm e}/(r)/\rho(r)](L/L_\odot)(M/M_\odot)^{-1}. \tag{2}$$

In this expression only the radiative acceleration due to Thomson scattering is considered, whereas the additional terms due to the hydrogen and helium continua, which may not play a decisive role in the case of P Cygni (see Lamers, 1986), are neglected. The self-consistently calculated sets of line force parameters, $k(r)$, $\alpha(r)$, $\delta(r)$, which enter also in Eq. (1), are introduced by the concept of the force multiplier (see Papers I, III and IV).

Our assumption that P Cygni lies close to the Eddington-limit is also supported by the small terminal velocity of this object: a high value of Γ which enters the formula for the escape velocity,

$$v_{\rm esc}^2 = \frac{2GM_*}{R_*}(1-\Gamma(R_*)) \tag{3}$$

yields a small value of $v_{\rm esc}$ and, consequently a small value of v_∞, since $v_{\rm esc}$ is related to v_∞ (see Abbott, 1978; and for the non-linearity of this relation Paper VII and Kudritzki et al., 1989 (Paper VI)).

3.1. The dependence of $\dot{M}$ on the proximity to the Eddington-limit

Equation 1 shows the dependencies of $\dot{M}$ on Γ and on the force multiplier parameters (k, α and δ), which represent the influence of the dynamical properties via the line acceleration. However, the absolute magnitude of $\dot{M}$ and the slope of the $\dot{M}$ vs. Γ relation have not yet been defined. In order to study this in detail we proceed in two steps.

First, the dependence of M on Γ is investigated separately by means of a treatment, in which calculated sets of (k, α, δ) are kept fixed over the range of $\Gamma(M_*)$: these values were then applied to the model sequence for $T_{\rm eff} = 19\,300$ K, $\log L/L_\odot = 5.74$ (see Fig. 1). Figure 3a shows the mass-loss rates computed using two self-consistent sets of parameters, obtained for a model from the low mass side and for one from the high mass side of the grid, along $\Gamma(M_*)$.

It is readily seen that $\dot{M}$ in fact increases strongly with Γ along the sequence of *constant luminosity* and that the slopes of the two curves are nearly identical. Furthermore, apart from the encouraging result that the observed mass-loss rate for P Cygni lies just between these two curves, the most significant feature of Fig. 3a is the large gap between the curves, which covers a range of nearly one dex in $\dot{M}$. The two curves were obtained from the self-consistent calculations of a model with high Γ ($\Gamma = 0.8$, upper curve) and one with a somewhat lower value ($\Gamma = 0.6$, lower curve), respectively. This implies that some physical process which has obviously a dramatic influence on the dynamical properties of the wind is initiated for a small increase of Γ.

As a second step, we have carried out fully self-consistent calculations, i.e. with self-consistent, interval dependent (k, α, δ), using the correct electron density dependence for the calculation of Γ, and a temperature structure taken from Drew (1985) for each model of the $\log L/L_\odot = 5.74$ sequence (see Table 1). Rather surprisingly, these calculations show a strong discontinuity in $\dot{M}$ rather than a gradual transition from the low to the high $\dot{M}$ curve, which reveals a sort of *bi-stability* for the wind of P Cygni (see Fig. 3b). An additional striking feature of Fig. 3b is that the discontinuity occurs exactly in the range of the $M-L$ relation predicted by MM and hence yields a mass loss rate comparable to the observed value. The conclusion that this discontinuity is related to the instability mechanism working in P Cygni (see below) is supported by additional model calculations for the tracks with $T_{\rm eff} = 19\,300$ K, $\log L/L_\odot = 5.97$, 5.86, since from these calculations it is obvious that the discontinuity is a common feature obtained for each of the luminosity sequences of Fig. 1 (see Fig. 4).

We have seen above that only the models which lie close to the $M-L$ relation of MM yield mass-loss rates close to the observed

© European Southern Observatory • Provided by the NASA Astrophysics Data System

1990A&A...237..409P

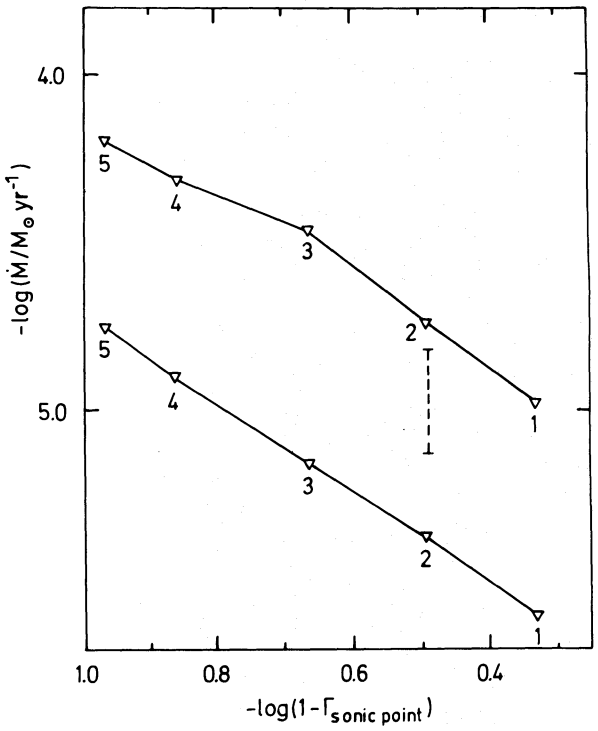

Fig. 3a. $\log(\dot{M})$ as a function of one minus the ratio of luminosity divided by Eddington luminosity obtained at the sonic point for the model sequence (see Fig. 1). The two curves show the $\dot{M}$ calculated for two fixed sets of the dynamical iteration values k, α, δ. These sets of values were obtained from the self-consistent calculations of a model with high Γ ($\Gamma = 0.8$, upper curve) and a model with a lower value of Γ ($\Gamma = 0.6$, lower curve). The vertical dashed line indicates the observed mass-loss rate for P Cygni

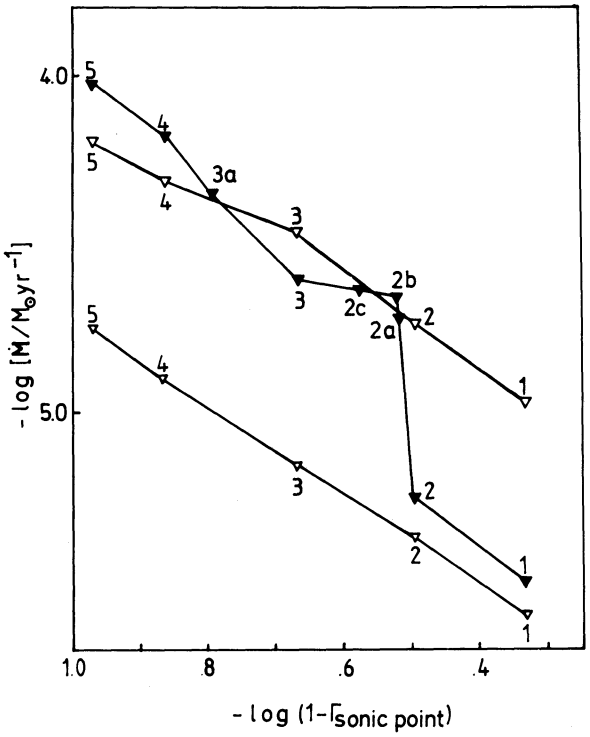

Fig. 3b. $\dot{M}$ vs. $(1-\Gamma_{s.p.})$. The curves shown in Fig. 3a (open symbols) are compared with the results from self-consistent calculations obtained for each model of the $\log(L/L_{\odot}) = 5.74$ sequence (filled symbols). These calculations reveal a strong discontinuity rather than a gradual transition from the low to the high $\dot{M}$ curve

values. This indicates that the comparison between the calculated and the observed mass-loss rates places additional constraints on the mass of P Cygni. This is shown in Fig. 5, where we have plotted the real observable quantity, which is $\dot{M}/v_{\infty}$ in the case of P Cygni. We see that with this presentation, the discontinuities fit also the observed $\dot{M}/v_{\infty}$ value and the Γ value predicted for P Cygni using MM's tracks for $T_{\rm eff} = 19\,300$ K.

Moreover, the results of our calculations for the second set of model sequences corresponding to $T_{\rm eff} = 18\,300$ K (see Table 1) show that none of these models is consistent with the observed wind dynamics (see Table 3). This also places constraints on the effective temperature and thus on the knowledge of the interstellar extinction for P Cygni (see Sect. 2).

In Table 3 the dynamical results of the models with constant temperature and of those with Drew's (1985) temperature structure can also be compared.

3.2. The bistability of the wind of P Cygni

In the previous section we have seen that in the domain of stellar parameters relevant for P Cygni the wind is bi-stable, and sensitive to very small changes of either R or L ($\Delta R/R > 1.5\%$ or $\Delta L/L > 3\%$). Although we will later present a possible explanation of how these photospheric changes can be stimulated, we first consider the reason for the jump in $\dot{M}$, since this follows directly from our calculations.

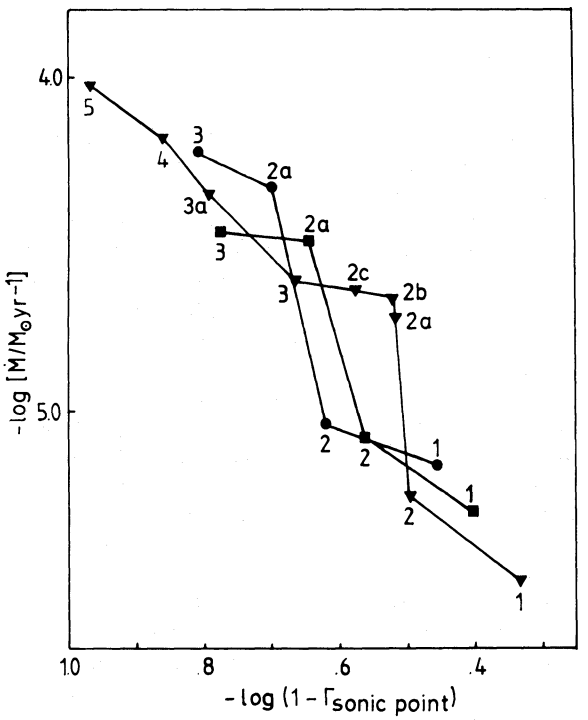

Fig. 4. $\dot{M}$ vs. $(1-\Gamma_{s.p.})$ for the tracks of constant L shown in Fig. 1. This diagram confirms the bi-stability for the wind of P Cygni (see Fig. 3b – for a discussion see text)

© European Southern Observatory • Provided by the NASA Astrophysics Data System

1990A&A...237..409P

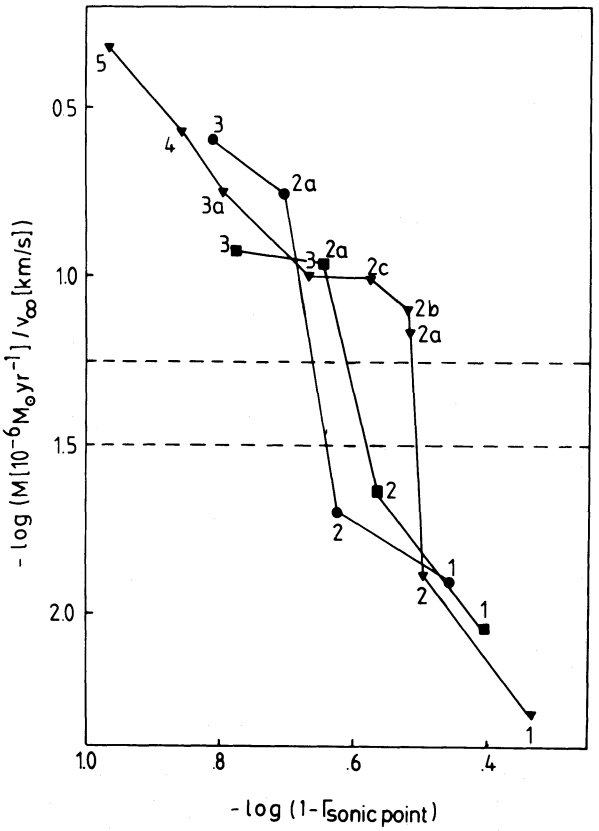

Fig. 5. The real observable quantity $\dot{M}/v_\infty$ as a function of $(1-\Gamma_{s.p.})$ for the three sequences of selfconsistent models (see Fig. 1 and 4). With this presentation it is shown that the discontinuities fit also the observed $\dot{M}/v_\infty$ value (dashed horizontal lines)

The mechanism, which causes an enormous change in the wind density, is related to the behaviour of the Lyman continuum. This can be understood from the well known fact that in stellar winds the hydrogen or helium continuum becomes suddenly optically thick when a critical value of mean wind density, effective temperature, or electron temperature at the base of the wind is reached (see for instance Paper III, Gabler et al., 1989, Hillier, 1987, private communication, Pauldrach et al., 1989a, Schmutz et al., 1989, private communication). This has drastic consequences for the ionisation stages of metals whose ground state photoionisation edges lie beyond the Lyman edge, because most of the flux is blocked in this frequency region by the high hydrogen opacity. As a consequence a shift to lower ionisation stages occurs. If we move now in Fig. 3a from the models with high masses and small Γ, which exhibit moderate mass-loss rates, and always show an optically thin Lyman continuum, whether or not a temperature structure is assumed, towards models with lower masses and higher Γ, $\dot{M}$ increases according to the $(1-\Gamma)$ dependence (see Fig. 3a). However, as soon as a critical mean density is reached at a certain critical Γ-value, the hydrogen continuum suddenly becomes optically thick, so that metals shift to lower ionisation stages. As will be shown below, these lower ionisation stages give rise to an enhancement of the radiative line acceleration, which finally produces the jump in $\dot{M}$.

3.2.1. Control of the line force by the Lyman continuum

As we have seen above, one of the essential steps for the back reaction of the Lyman continuum on the line force to occur is the change of the ionisation ratios of the metals. Figure 6 shows the ionisation fractions of S (II, III), Si (II, III) and C (II, III) the elements for which we obtained the largest differential deviations, over the whole wind range, for models 2 and 2b ($T_{\rm eff}=19\,300$ K, $\log L/L_\odot = 5.74$, see Table 1), which lie respectively before and after the discontinuity, (see Fig. 3b). The comparison shows an enhancement of up to 3 dex for the single ionised stages in the case of the high $\dot{M}$ model. Of course, this causes also a change in the distribution of the line force over the most important ionisation stages (see Fig. 7). The striking feature of Fig. 7 is that while the contribution to the force increases from singly to doubly ionised species for model 2, the opposite holds for model 2b. However, it is not yet clear whether in this case the shift to lower ionisation stages produces an increase of the *total* line force, which must be responsible for the significant enhancement of the mass-loss rate. In order to investigate this precisely, in Fig. 8a the flux weighted number of lines stronger than 10 times the Thomson scattering opacity per 2 Å interval is shown for model 2b as a function of wavelength. The graphical presentation in Fig. 8b shows the reduction of the line force from model 2 compared to model 2b, when the line force from model 2 is rescaled on the density and velocity structure of model 2b. In this figure then, the resulting ratio of flux weighted numbers of lines between model 2 and model 2b is shown. It is immediately seen that the line force of the model with the optically thin Lyman continuum (i.e. model 2) is in fact smaller by about 15%. This behaviour initiates the 'runaway' process which finally results in the state at the lower end of the discontinuity.

In addition to the total line force it is also of great importance to know how much of the acceleration is provided by optically thick lines. Lamers (1986) has argued, from an estimate of the radiative force, that weak lines are the most likely to be responsible for the acceleration of P Cygni's wind (cf. Sect. 2). This is not confirmed by our calculations. As is also indicated by Fig. 8a, our results show that some 50 to 60% of the line force is provided by optically thick lines, where the lower limit corresponds to models with small $\dot{M}$ (e.g. model 2) and the upper limit to models with high $\dot{M}$. This confirms our preliminary result of Sect. 2, where we obtained a similar ratio of optically thick and optically thin lines by assuming empirical velocity laws. Since we showed in Sect. 2 that such a ratio is not compatible with a linear velocity law, we can stress again, on the basis of our self-consistent calculations, that in the case of P Cygni a linear velocity law cannot be obtained by means of radiative acceleration.

3.3. The bistability as an origin of shell ejection

As we have already outlined in Sect. 1, P Cygni shows, besides its quiescent wind features, irregular variations of the line profiles in the visual and in the UV. (A complete list of references is given by van Gent and Lamers, 1986, we refer only to the recently obtained high resolution spectrograms of Markova and Kolka, 1984 in the visual and Lamers et al., 1985 in the UV.) This strongly suggests the hypothesis of shell ejection. However, despite the great efforts in this direction, our insight into the mechanism that causes shell ejection is still poor. As a result of an extensive study van Gent and Lamers (1986) have found that the variations of the line

© European Southern Observatory • Provided by the NASA Astrophysics Data System

1990A&A...237..409P

Table 3. Computed mass-loss rates and terminal velocities for models corresponding to the $M-L$ relation for post-RGB objects. The values in brackets are obtained for constant temperature structures ($T_e = T_{eff}$). The dashed line indicates the position of the discontinuity

T_{eff} (10^3 K)	$\log(L/L_\odot)$	$M/M_\odot$	$\dot{M}$ ($10^{-6} M_\odot\,yr^{-1}$)	v_∞ ($km\,s^{-1}$)	v_∞/v_{esc}	$\dot{M}/v_\infty$ ($10^{-8} M_\odot\,yr^{-1}$) ($km\,s^{-1}$)
		24.5	2.5	690	2.7	0.36
		* 19.5	5.3	400	2.1	1.33
			(4.0)	(440)		
		18.8	18.0	270	1.5	6.67
	5.74	18.3	21.7	267	1.5	8.13
		17.5	23.8	240	1.5	9.92
		16.5	24.5	236	1.6	10.38
			(33.0)	(330)		
		15.5	44.5	230	1.9	19.36
		15.0	64.0	225	2.0	28.44
		14.5	92.0	193	2.0	47.67
		28.5	4.2	620	2.6	0.68
		* 23.5	8.4	370	2.1	2.27
			(6.6)	(614)		
		22.5	32.0	285	1.8	11.23
19.3	5.86	20.5	32.5	275	2.1	11.82
		34.0	6.2	580	2.5	1.07
		* 29.0	9.2	450	2.6	2.04
			(7.7)	(675)		
	5.97	27.5	46.7	265	1.7	17.62
		26.0	58.0	225	1.7	25.78
		* 16.0	2.3	400	2.0	0.58
			(1.8)	(317)		
	5.6	14.0	5.0	280	1.6	1.79
			(4.0)	(550)		
		12.5	5.3	320	2.3	1.66
			(6.4)	(400)		
18.3	5.7	* 18.8	3.8	340	1.8	1.12
			(3.6)	(620)		
		16.8	5.6	300	1.9	1.87
			(5.1)	(500)		
	5.8	* 21.6	5.5	360	2.0	1.53
			(4.0)	(660)		

* Exact $M-L$ relation according to Maeder and Meynet (1987)

profiles are not due to periodic oscillations but to the irregular ejection of about 5 to 6 shells per year, which corresponds to a *mean time scale for ejection of about 60 to 75 days*. Since this result is in qualitative agreement with the time scale of non-radial pulsations for LBV's, they conclude that this might be the mechanism triggering shell ejection. Still, the values for the basic parameters of the shells are known only to within large uncertainties. Waters and Wesselius (1986) have found that a shell with a *density increase of a factor 5 located between 15 R_* and 50 R_** can explain the observed bump in the IR fluxes at 60 and 100 μm. Lamers (1986a) gave an estimate of ($5\,10^{-6} - 5\,10^{-5}$) $M_\odot\,yr^{-1}$ for the average mass loss rate due to shells. Moreover, variations in the radio flux (van den Oord et al., 1985) indicate a sudden recombination of the radio emitting region, which is explained by thick shells that block the ionising flux from the photosphere (see Lamers, 1986a).

© European Southern Observatory • Provided by the NASA Astrophysics Data System

1990A&A...237..409P

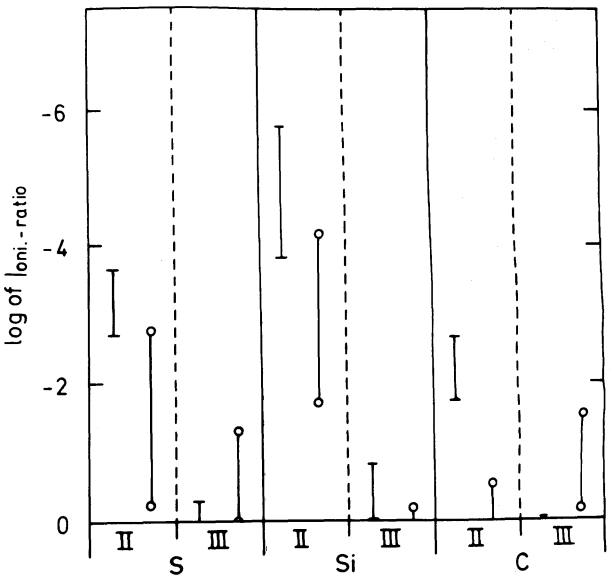

Fig. 6. For the models 2 (marked by horizontal bars) and 2b (marked by open circles) ($T_{eff} = 19\,300$ K, $\log(L/L_{\odot}) = 5.74$) the ionization fractions of S, Si and C are shown for the ionisation stages II and III averaged over the whole extend of the wind (vertical bars). (For a detailed discussion see text)

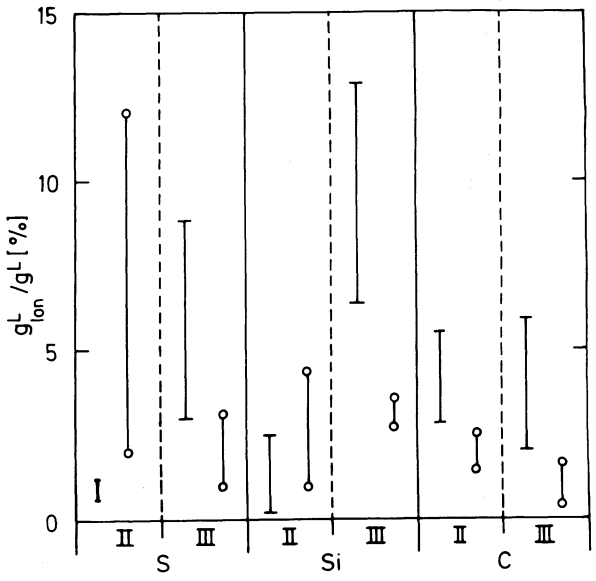

Fig. 7. Distribution of the line force contribution of the ionisation stages II and III of S, Si and C for the models 2 and 2b. For the presentation see Fig. 6. For a discussion see text

In view of our detection of the bistability mechanism, at least the last two observational features are naturally explained, if one accepts that the shell phase occurs when the star lies at the upper curve of the discontinuity (see Fig. 3b) and that the quiescent phase corresponds to positions somewhat above the lower curve. (We should remind the reader at this point that the curves in Fig. 3 and 4 may shift towards higher $\dot{M}$, if the radiative acceleration due to the hydrogen and helium continuum and multi-line effects (see below) are properly taken into account.

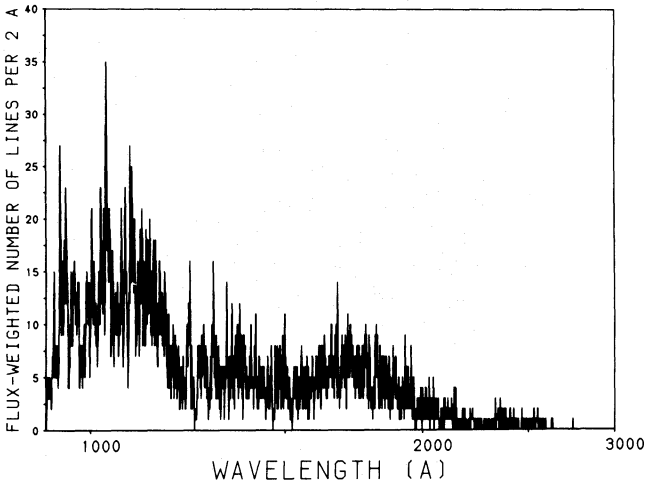

Fig. 8a. Model 2b: Number of lines stronger than 10 times the Thomson scattering opacity, per 2A interval and weighted by $H_\nu dv/H$

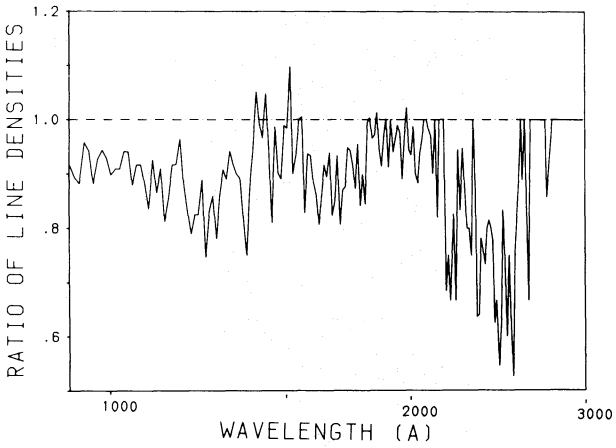

Fig. 8b. The ratio of flux-weighted number of lines (as in Fig. 8a) of model 2 and model 2b versus wavelength. For reasons of differential comparison, the line-strengths of model 2 were rescaled on the density and velocity structure of model 2b

Therefore, our calculations are still uncertain, but, since these two effects operate in opposite directions the net effect can be expected to be small.)

Nevertheless, although we know (see Sect. 3.2) that the mechanism causing the bi-stability can be activated by small changes in radius or in luminosity, we still have no explanation as to how the mechanism can be triggered. It is clear, however, that changes of the stellar parameters cannot be initiated by the behaviour of the outflowing part of the envelope alone as long as the wind is optically thin in the visual, which is obviously the case for all the models we calculated.

On the other hand it is known that the wind albedo (i.e. the back-scattering of radiation onto the photosphere from the supersonic region) can change the temperature structure considerably in the outermost part of the photosphere via the so-called wind blanketing effect (see Abbott and Hummer, 1985).

© European Southern Observatory • Provided by the NASA Astrophysics Data System

1990A&A...237..409P

Because of the observed huge line blocking factor (about 0.4, see Lamers et al., 1983, Lamers, 1986), the effect of wind blanketing seems to be essential in order to explain the behaviour of P Cygni. A change in the amount of back-scattered radiation will result in a change of the temperature structure in the layers where the continuum is formed. This change in the albedo, which is illustrated in Fig. 9 for models 2 and 2b, can be triggered by two connected processes: A change of the ionisation ratios arising from the sudden change of the optical thickness in the Lyman-continuum encountered in the range of the discontinuity, will enlarge the number of backscattering lines and also increase the line force. The correlated increase of mass loss and density will then account for a significantly enhanced albedo by continuum processes (mainly Thomson scattering), which is clearly shown by the offset of the two curves of Fig. 9 in the region of low line density beyond 2500 Å. As a comparison to observations, Fig. 10a shows the *emergent* flux for models 2 and 2b, and the low resolution energy distribution of P Cygni (from Lamers et al., 1983, Fig. 4). It is obvious that our models represent the major features (especially the large Fe III complex ($\lambda\lambda$ 1887–2098) very well. It is interesting to note that nearly all lines are actually formed in the wind, whereas only for a few lines (e.g. Si III $\lambda\lambda$ 1206.5, 1294–1298, C IV 1248, 1251) the photospheric component is missing due to our present treatment.

Furthermore, the *measured* flux blocking factor of P Cygni (Fig. 10b) lies between those calculated from our two models (although nearer to the optically thick case), which strengthens our previous conclusion concerning the relation between the occurrence of the shell phase and the position of the star. (Only in the region between 2000 and 2400 Å a difference occurs due to the neglection of *photospheric* line blocking in our models, whereas the blocking for $\lambda > 2500$ Å given by Lamers et al. seems a bit too large, and is in our opinion due to an overestimated continuum).

From the discussion above, we propose a circular mechanism based on the results of our study, which would operate as follows: When $\dot{M}$ switches towards the upper curve of Fig. 3 the albedo increases with the expansion of the high density region due to the increase of the correlated line force, and the photospheric temperature increases accordingly. If the photospheric temperature becomes larger than a certain critical value – which is the case if the albedo is mostly controlled by the high $\dot{M}$ region –, the high temperature causes hydrogen to be strongly ionised, thus giving rise to a decrease of the line force (see above) and, hence, to a decrease of the backscattered photons. $\dot{M}$ switches then back towards the lower curve of Fig. 3, and this in turn decreases the temperatures at the base of the wind. Now again, if the albedo is mostly controlled by the low $\dot{M}$ region – which is the case when the preceding "shell" has left the acceleration part of the wind –, the photospheric temperature decreases below a certain critical value and, therefore, $\dot{M}$ switches towards the upper curve of Fig. 3. In other words, an increase of wind column density leads to an increase in the wind blanketing, which leads in turn to an increase of the photospheric temperature, which produces a reduction of the mass loss rate, which in due course produces a reduction in the wind column density, whereafter the same causal chain repeats with the opposite sign.

This process causes quasi-periodic relaxation oscillations, where it remains to be shown that the observed shell-ejection rate and the spatial extension of the shells are at least in rough agreement with the proposed mechanism.

An upper limit for the spatial extension of a shell can be obtained from our argument that $\dot{M}$ switches towards the lower side of the discontinuity only if the wind blanketing is controlled by the high density region, since this requires that the high $\dot{M}$ regime (i.e. the shell) becomes so extended that it coincides with the major back-scattering part of the envelope, whose outer radius is located at approximately $5\,R_*$ in the case of P Cygni. (For larger radii the albedo drops below 1% and becomes negligible.) The extension which is given by this upper limit is consistent with the observational requirements cited above. The lower limit is simply given by the sonic point as the boundary between the photospheric and the wind regime.

The rate of shell ejections follows now directly from the time scale for a cycle of the described mechanism. Since a density switch occurs only if the major back-scattering part of the wind ($R_{\rm sound} - 5\,R_*$) is dominated by a single mode of the bistability, the time scale can be determined by an estimate of the time interval which is required for each mode to propagate through the acceleration region. This time interval can easily be derived by the assumption of a β-velocity law, and is given by

$$\Delta t = \frac{R_*}{v_\infty} \int_{R_{\rm sound}}^{5} \frac{dr}{(1-b/r)^\beta} \,. \tag{4}$$

Using the values $R_* = 76\,R_\odot$ (see Sect. 4), $v_\infty = (206-300)$ km s^{-1} $\beta = 4$, $R_{\rm sound} = 1.8$, $b = 0.859$ for the velocity field discussed in Sect. 2, this yields $\Delta t = (28–35)$ days, whereas with the values obtained from our current best model (see Sect. 4, $R_{\rm sound} = 1.34$, $b = 0.63$, $v_\infty = 195$ km s^{-1}) a value of $\Delta t = 38$ days is implied. Since the ejection of a shell occurs once every cycle, when the albedo is small, the time-scale between successive shell ejections is twice Δt, so that a rate of 5 to 6 shells per year is found, in agreement with the observed number.

The qualitative agreement which we have found between the basic observational features of the shell ejection and the behaviour of the self-activated bi-stability mechanism is, of course, encouraging, since we have not only understood the way in which changes of the mass-loss rate occur, but also the way in which the photosphere reacts to these changes. However, the present work is only a first step because we are not able, for the time being, to

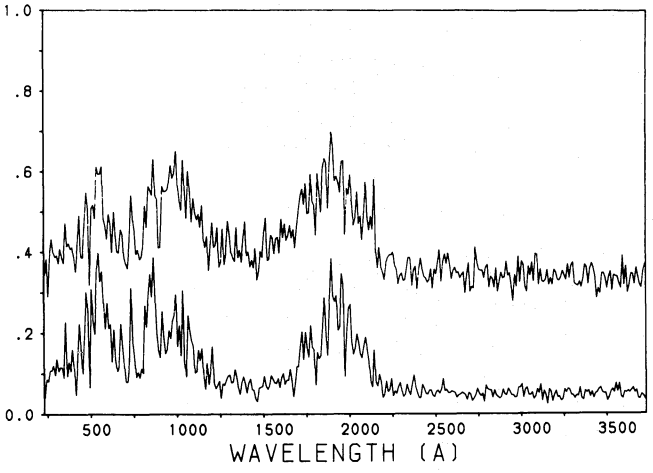

Fig. 9. The albedo (at sonic point) for model 2b (upper) and model 2 (lower curve) in the range 228–3728 Å. Calculation via Monte-Carlo method (cf. Paper IV); the applied resolution is 10 Å

© European Southern Observatory • Provided by the NASA Astrophysics Data System

1990A&A...237..409P

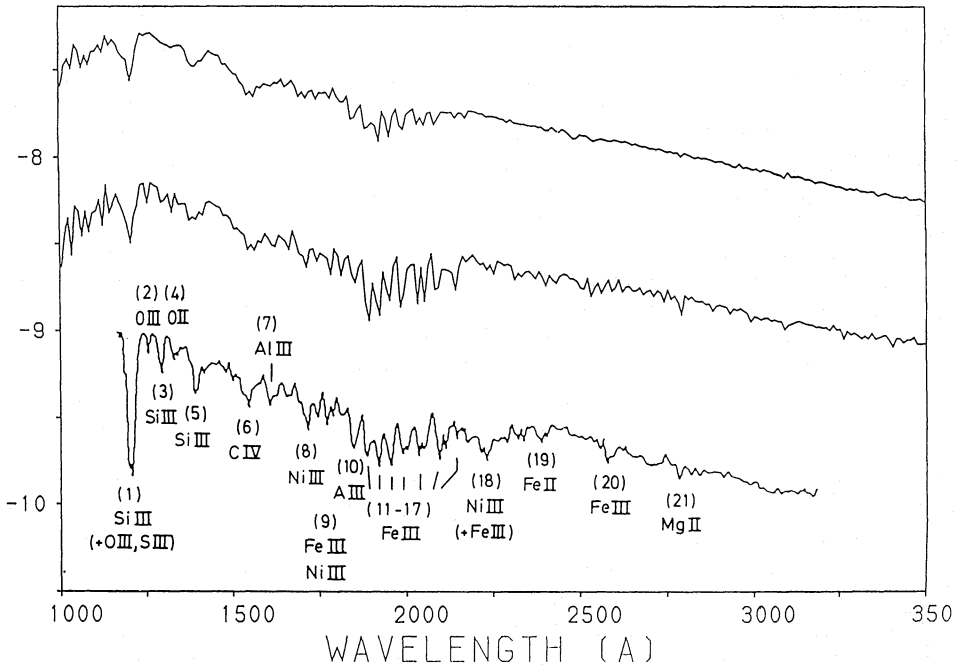

Fig. 10a. Calculated UV energy distribution for P Cygni in units of erg cm^{-2} s^{-1} Å^{-1}. Upper curve: model 2, middle: model 2b, bottom: observations (from Lamers et al., 1983). For convenience, the upper curve is shifted upwards by +1.0 and the lower curve downwards by −1.0. The applied angular diameter is 0.41 10^{-3} arcsec (cf. Sect. 4). Line identification (RL = resonance line): (1) Si III (1206.5, RL); (2) O III (1247.4); (3) Si III (1294.98); (4) O II (1335); (5) Si III (1417); (6) C IV (1548.51, RL); (7) Al III (1611.9); (8) Ni III (1709/15); (9) Fe III/Ni III (1784/90); (10) Al III (1855, RL); (11–17) Fe III (1887, 1922, 1959, 1992, 2020/37, 2090/98, 2152); (18) Ni III (+Fe III), (2227/33); (19) Fe II (2382/95, RL); (20) Fe III (2583), (21) Mg II (2795)

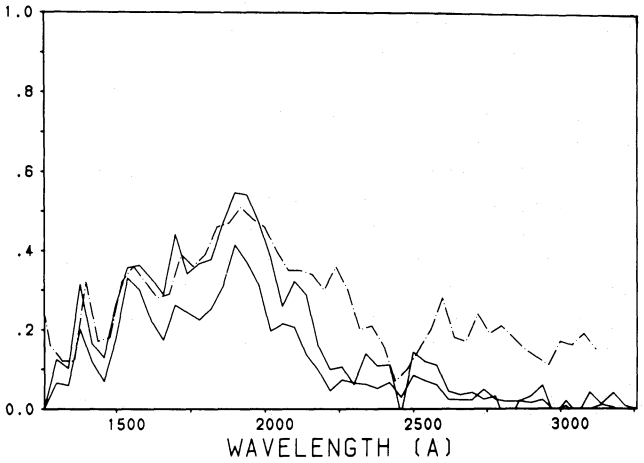

Fig. 10b. Line blocking factors for model 2b (upper) and model 2 (lower curve). For comparison, the observations by Lamers et al. (1983, 40 Å resolution) are given by the dashed-dotted curve

describe the changes undergone by the photosphere quantitatively. This would require at least the introduction into our treatment of the effects of line blocking and line blanketing in a realistic way. Although this is an additional complex problem (thousands of lines have to be considered), the work on this refined theory is under way in our group.

4. The current best model

The effects of line overlap have been neglected in our calculations up to now. This was justified, since so far we have mainly discussed the mass loss rate, which is expected to be described better when multiline effects are not considered. The reason for this assumption is simple: the mass-loss rate is determined in the sub-sonic part of the envelope, where the enhancement of the radiative acceleration due to the H and He continua (see Lamers, 1986) is almost cancelled by the reduction of the line acceleration due to multi-line effects (see Puls et al., 1989). Since the enhancement of the continuum has been neglected, the error introduced is approximately balanced by the neglection of the multiline effects. However, in this section we would like to examine the extent to which our calculations are able to reproduce the observed terminal velocity and the velocity structure precisely. It is therefore necessary, in view of the strong line blocking occurring in the wind, to take the line overlap into account. This will lead to a significant reduction of the line force in the upper part of the envelope, which might be crucial for determining accurately the slope of the velocity law. However, such self-consistent calculations are made difficult by the fact that P Cyg lies within the range in which the mass loss function is discontinuous. Hence, instead of self-consistent calculations, which would result in an alternating iteration cycle due to the discontinuity, we prepared consistent models. This was done by choosing sets of *f*orce-*m*ultiplier *v*alues (FMV) for which we ran a complete stellar wind model. In the cases where the resulting FMV were not consistent with the starting values we adjusted the latter and proceeded again until convergence was reached. The obvious advantage of this time-consuming procedure is that the calculations are not hampered by the alternating process of the hydrodynamics.

These calculations were performed in the range of the discontinuity of all three tracks corresponding to $T_{\rm eff} = 19\,300$ K corresponding to the results of Sect. 3.1 (see also Table 3). However, our investigation of IR and radio data provides some rather tight limitations on the stellar and wind parameters. Firstly the *observed* optical, far-IR and radio fluxes can be *consistently* reproduced – i.e. assuming the same ratio of $R_*/d = \Theta$ – only by models with

$$\dot{M}/(v_\infty R_*^{3/2}) = \text{const.}$$

© European Southern Observatory • Provided by the NASA Astrophysics Data System

1990A&A...237..409P

This follows from the scaling relation of the optical depth for longer wavelengths (ff+bf processes, neglecting Thomson scattering, see. e.g. Lamers and Waters, 1984). Although those models will yield almost identical fluxes in the above wavelength range, one may then have to accept a different distance for the object under consideration. The distance of P-Cygni is well determined: $d = 1.8 \pm 0.1$ kpc (see Lamers et al., 1983). A change in the photospheric radius from 76 to 66 R_* e.g. leads to a reduction of the distance to 1.56 kpc, which lies well outside the tolerable limits.

Although it is possible to construct models with same ratio $\dot{M}/v_\infty$ for different stellar radii by adopting different masses (cf. Table 3), for P-Cygni we have to accept a definite terminal velocity of about 200 km s^{-1} (with an unlikely upper limit of 300 km s^{-1}), which, in connection with the radio data, gives a definite (relatively narrow) range of mass losses. It is evident that only few out of the numerous models from Table 3, if any at all, will yield wind parameters in this range.

Even more striking is the constraint on the velocity field. As proved in Sect. 2, this has to be extremely flat (comparable to a parameter $\beta \approx 4$) to reproduce the observed *near IR*-excess as well.

Out of the many models calculated on the three tracks with $T_{\rm eff} = 19\,300$ K, only one model was able to reproduce all the features discussed simultaneously. This *current best model* has stellar parameters $R_* = 76\,R_\odot$ and $\log(g) = 2.04$ – *corresponding to a mass of 23* $M_\odot$.

The wind structure of our current best models is defined by $\dot{M} = 12.1\,10^{-6}\,M_\odot\,{\rm yr}^{-1}$ and $v_\infty = 195$ km s^{-1}, where the velocity field and density stratification is given in Fig. 11. Note that at $r = 100\,R_*$ only 72% of the terminal velocity is reached. Figure 12 compares the resulting IR-flux to the observed one, where the best fit was obtained for an angular diameter of $\Theta = 0.41\,10^{-3}$ arcsec, which lies well inside the range given by Lamers et al. (1983), $\Theta = (0.39 \pm 0.08)\,10^{-3}$ arcsec. With $R_* = 76\,R_\odot$, the distance results in $d = 1.72$ kpc.

A detailed comparison of the spectral features (both UV + optical) will be given in a forthcoming paper when

i) the up to now missing line blocking calculations (wind + photospheric) are incorporated into our code (allowing also for the inclusion of photospheric components),

ii) the UV observations ($\sim$60 different done by IUE) are studied in detail and

iii) new observations in the optical part of the spectrum (where some of the most interesting P-Cygni features are situated) are performed by our group.

4.1. *Error estimates*

From the discussion outlined in the preceding sections, it is obvious that the complete stellar parameter set depends exclusively on the position of the bifurcation between low and high mass loss rate, as the observed rate lies just in between.

From the combined analysis of radio and IR data in connection with the well-defined distance (see above), we estimate the maximum error in stellar radius to be $\pm 4\,R_\odot$. (The reader may note, however, that at present it seems rather difficult to construct wind models for this range which are *actually* capable of reproducing both the IR and radio measurements). A subsequent interpolation of the values given in Table 3 yields a variation of the position of bifurcation as a function of stellar radius to occur

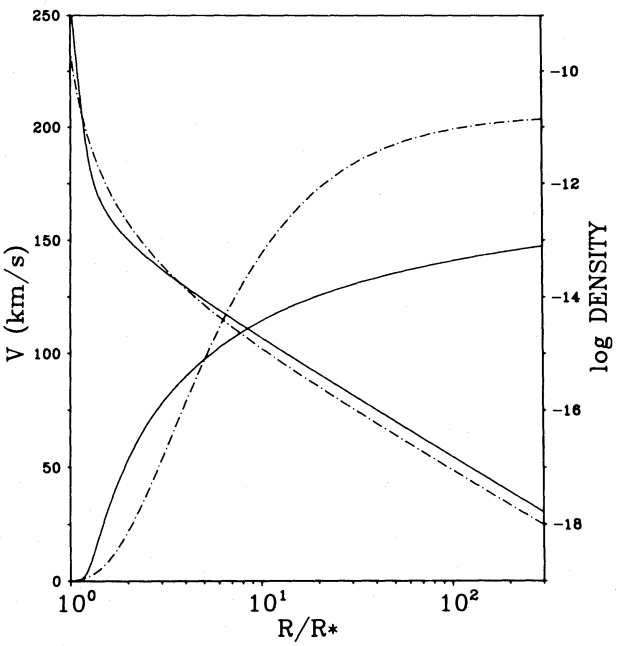

Fig. 11. The current best model: velocity and density stratification. For comparison, the same quantities are given for the $\beta = 4$ velocity law (dashed-dotted, see Sect. 2)

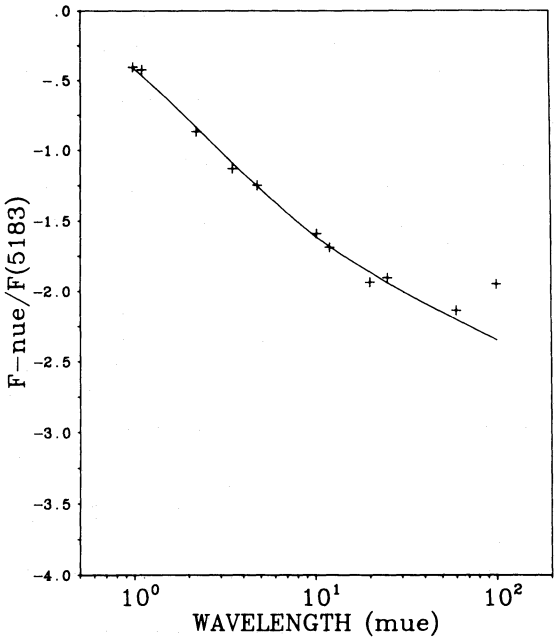

Fig. 12. The current best model: comparison between calculated and observed IR-flux (see also Fig. 2b)

at $M_* \approx 21\,M_\odot$ ($R_* \approx 72\,R_\odot$) and $M_* \approx 25\,M_\odot$ ($R_* \approx 80\,R_\odot$). Therefore, a (rather pessimistic) error assessment is

$R_* = 76 \pm 4\,R_\odot$, $M_* = 23 \pm 2\,M_\odot$, $\log g = 2.04 \pm 0.01$.

With respect to the wind parameters the errors remain identical to the observational constraints for the following reasons: Although there is an almost unique solution for the wind

© European Southern Observatory • Provided by the NASA Astrophysics Data System

1990A&A...237..409P

structure for given stellar parameters, consistent with the observations (in the assessed error ranges), here the influence of the chosen temperature profile becomes decisive: Although the position of the bifurcation is not modified, we find from Table 3 (calculations with Drew's temperature stratification or with constant T_e, respectively) differences in the absolute values (mainly the mass loss). In this sense, it is absolutely possible to obtain different wind parameters (although in consistency with observations) for a modified $T_e(r)$ *and* slightly different gravity. However, it should be pointed out again that all such minor modifications have no influence on the general features, unless the structure of the bimodality remains as steep as was found in Sect. 3.1.

5. Conclusions and future work

Taking P Cygni, the prototype of the group of "P Cygni type variables", as an example, we have carried out a systematic investigation of the basic properties of objects located close to the Humphreys-Davidson limit at the top of the HR-diagram. For this investigation, calculations have been performed using our self-consistent stellar wind code, for a large grid of wind models necessary to represent the range of stellar parameters that could represent the uncertain evolutionary stage of P Cygni in its quiescent phase. On the basis of these calculations we have determined constraints on the evolutionary stage and on the stellar parameters of this star. We have shown that not only the acceleration of the wind but also the observed set of dynamical parameters is explained completely by radiation pressure due to electron scattering and to some 80 000 line transitions. We have also demonstrated that P Cygni's wind is highly unstable with respect to extremely small photospheric changes, which result in a drastic enhancement of the mass-loss rate and cause the object to 'jump' across the discontinuity. We also found that, on the basis of this bi-stability, a self-triggered mechanism occurs which appears to explain the variability of P Cygni's "quiescent" wind, and that the basic observational features of the shell ejection are in quantitative agreement with this mechanism.

We have presented what is currently our best model, which yielded from the consistently calculated hydrodynamics a mass-loss rate ($\dot{M}=12.1\,10^{-6}\,M_\odot\,\mathrm{yr}^{-1}$) and a terminal velocity ($v_\infty=195\,\mathrm{km\,s}^{-1}$) that reproduce the observed values. Since this was the only model which fitted also almost perfectly the IR excess observed from the derived velocity structure, we can in addition set the stellar parameters for P Cygni with a high degree of accuracy to $\log L/L_\odot=5.86$, $\log g=2.04\pm0.01$, $R_*=76\pm4\,R_*$.

Hence, P Cygni's mass ($M=23\pm2\,M_\odot$) is *no longer* a highly uncertain parameter. Here it is also interesting to notice that P-Cygni has a spectroscopic twin, the *eclipsing* binary R81 in the LMC. Wolf et al. (1981) determined the stellar parameters of this object to be $T_{\mathrm{eff}}=20\,000\,\mathrm{K}$, $M_{\mathrm{bol}}=-10$ and $R_*=70\,R_\odot$. In a detailed analysis of phase dependent high dispersion high S/N spectra Stahl et al. (1987) showed that the mass of the combined system is about $33\,M_\odot$, with a (more uncertain) mass ratio of $M_1/M_2=3$, which yields for the primary $M_*=25\,M_\odot$, a value very close to our conclusion for the mass of P Cygni.

From our results we can first of all conclude that the concept of radiation driven cool winds is the right way to describe in a quantitatively proper way not only the stationary wind dynamics of objects at the top of the HR-diagram, but also the variability due to shell ejection. The second conclusion is that the wind properties offer an important tool for constraining the evolutionary status and determining the stellar parameters of objects which lie close to the Eddington-limit and the wind parameter of which depend strongly on the stellar parameters.

However, we regard our work only as a first step. The next steps will be the realistic inclusion of the effects of line blocking and line blanketing in our treatment, so that the reactions of the photosphere to mass loss changes due to the 'bi-stability' can be calculated quantitatively together with the rate of shell ejections and the amount of mass which is lost via this process; the investigation of whether the bi-stability mechanism is a common feature for all PCTs and thus for most of the LBVs, and the comparison of observed and calculated UV and visual wind spectra.

Moreover, it would be interesting to couple our stellar wind code with evolutionary calculations to investigate the formation of PCTs from massive O stars ($M_{\mathrm{ZAMS}}>40\,M_\odot$). In view of our present results a similar simple explanation may be found for the out-bursts as we found for the shell ejection. Our calculations have been performed for objects below the instability limit proposed by Humphreys and Davidson (1979, 1984) and since they have so far shown a huge dependence of $\dot{M}$ on the ratio of stellar to Eddington luminosity, such combined calculations might reveal a violent phase of mass-loss at this instability limit. Furthermore, such calculations should investigate whether the evolutionary tracks might be altered by the discontinuous behaviour of $\dot{M}$ in the range of the bi-stability.

Acknowledgements. We wish to express our thanks to our "Tai Pan" (Prof. Dr. R.P. Kudritzki) for helpful discussions and especially for strong motivation during the course of this work. It is also a pleasure to thank Dr. P.A. Mazzali and Dr. D.G. Hummer for the careful reading of the manuscript. Finally, we wish to thank Dr. H. etc. Lamers and Dr. J. Hillier for discussions when this work was still in a preliminary stage and the referees Dr. J. Castors and Dr. J. Drew for their useful comments. This research was granted under Ku 474/11-3 by the Deutsche Forschungsgemeinschaft. The calculations presented here were performed on a Cyber 995 of the Leibniz Rechenzentrum München which is to be acknowledged for supplying us with 2 MCPs computing time. We would also like to thank God, the Big Bang, Einstein and Feynman for making P Cygni available.

Appendix: velocity field and acceleration

Rewriting the equation of motion for radiatively driven stellar winds under the usual assumption (cf. Paper I), we obtain for *a given* velocity law

$$r^2 g^{\mathrm{L}}_{\mathrm{rad}}(r)=v_\infty^2/R_*\,r^2 v\,\mathrm{d}v/\mathrm{d}r\,[1-a^2/(v_\infty^2 v^2)]-2a^2 r/R_* + GM/R_*^2-r^2 g_{\mathrm{Th}} \qquad \text{(A1)}$$

where $v(r)$ in units of v_∞, r in R_*, a the isothermal sound speed and g_{Th} the acceleration due to Thomson-scattering. Taking into account the stellar parameters of our current best model – which differ only in the mass from that given by Lamers (1986) –, i.e. $T_{\mathrm{eff}}=19\,300\,\mathrm{K}$, $R_*=76\,R_\odot$ and $M_*=23\,M_\odot$, and using the wind parameters and linear velocity law (see Sect. 2) given by Waters et al. (1986), the radiative line acceleration as function of distance reads

$$r^2 g^{\mathrm{L}}_{\mathrm{rad}}(r)=0.26r^3+0.197r^2-0.429r+29.73. \qquad \text{(A2)}$$

© European Southern Observatory • Provided by the NASA Astrophysics Data System

1990A&A...237..409P

On the other hand, radiation driven wind theory predicts the line force to vary roughly according to

$$r^2 g^{\mathrm{L}}_{\mathrm{rad}}(r) \sim (r^2 v\, \mathrm{d}v/\mathrm{d}r)^{\alpha} v^{-\delta} \qquad \text{(A3)}$$

where the second term derives from the quantity $(n_e/W)^{\delta}$ in the force-multiplier concept (cf. Paper I). In case of a linear velocity law, (A3) breaks down to

$$r^2 g^{\mathrm{L}}_{\mathrm{rad}}(r) \sim r^{3\alpha-\delta}. \qquad \text{(A4)}$$

From Eq. (A2) it follows that

$r^2 g^{\mathrm{L}}_{\mathrm{rad}}(r) \sim$ const. for $r = 1 \ldots 3\,R_*$ $(v < 0.22 v_\infty)$

$r^2 g^{\mathrm{L}}_{\mathrm{rad}}(r) \sim r^3$ for $r = 3 \ldots 15\,R_*$

and a comparison with (A4) yields $\alpha \sim \delta/3$ in the inner and $\alpha \sim (1+\delta/3)$ $(|\alpha| \leq 1)$ in the outer part of the wind. With respect to the small value of δ this gives $\alpha \approx 0/1$ respectively. As the parameter α indicates the contribution of optically thick lines to the total number of lines (cf. Paper II), the above result implies that a "linear" wind should be driven by almost *only optically thin* lines in the *lower* and by almost *only optically thick* lines in the *outer* part of P-Cygni's atmosphere. As stated already in Sect. 2, this is in strong contradiction to the calculated NLTE line force *resulting from* the linear velocity field, which gave a mean value of $\alpha \approx 0.61$ throughout the wind. An even stronger counter argument from this discussion arises from the fact that the contribution of optically thick lines should be a *decreasing* function of radius, in contradiction to the situation considered above.

The same analysis can be carried out for $\beta = 4$ velocity field, which was found to be consistent with the observed IR excess as well. In this case, the parameter α necessary to build up the responsible line force must be of order $\alpha \approx 0$ $(r < 1.7\,R_*$, $v < 0.05\,v_\infty)$ and $\alpha \approx 0.7$ for $r > 2.5\,R_*$, whereas the *resulting* line force gives $\alpha \approx 0.68$, a situation which is much more promising. Figure 13 now shows the total outwards directed acceleration necessary for and resulting from the $\beta = 4$ law. Apparently, the calculated line force in single-line approximation is too large, whereas the inclusion of line blocking (cf. Paper IV) finally yields an "output" force very close to the applied "input" one. This result is a very encouraging one as it shows that most probable P-Cygni's wind is driven by mainly line pressure which gives rise to the typical, whenever rather flat β-structure of radiatively driven winds.

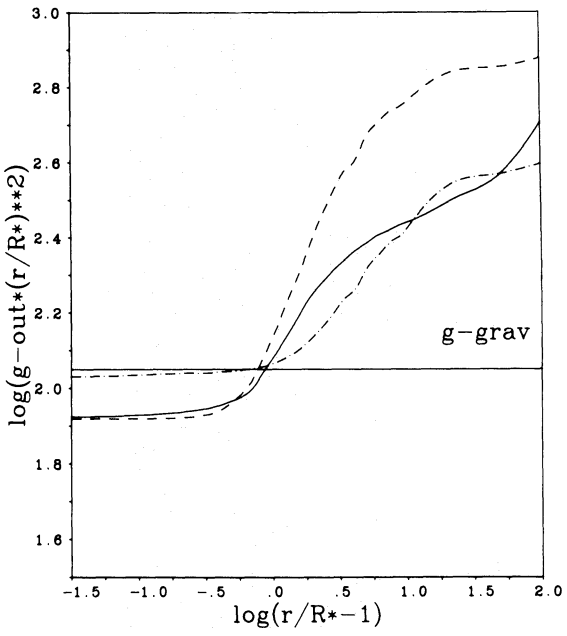

Fig. 13. Outwards directed acceleration $r^2 g_{\mathrm{out}}$, $g_{\mathrm{out}} = g^{\mathrm{L}}_{\mathrm{rad}} + g^{\mathrm{Th}}_{\mathrm{rad}} + 2a^2/r$, for the $\beta = 4$ velocity law (model parameters see text). Dashed-dotted curve: the acceleration *required* for building up the velocity structure; dashed curve: the acceleration *resulting* from the single-line approach; bold curve: the acceleration taking into account line blocking in the wind. (Radiation transport calculated with comoving frame formalism (see Paper IV)). Gravity ($\log(g) = 2.04$) is also indicated. Note that g-out = g-grav defines the sonic point

References

Abbott, D.C.: 1978, *Astrophys. J.* **225**, 893

Abbott, D.C.: 1982, *Astrophys. J.* **259**, 282

Abbott, D.C., Telesco, C.M., Wolff, S.C.: 1984, *Astrophys. J.* **279**, 225

Abbott, D.C., Hummer, D.G.: 1985, *Astrophys. J.* **294**, 286

Allen, C.W.: 1973, *Astrophysical Quantities*, 3rd ed., Athlone, London

Barlow, M.J., Cohen, L.: 1977, *Astrophys. J.* **213**, 737

Becker, R.H., White, R.L.: 1985, in "*Radio stars*", *Astrophysics and Space Science Library*, Vol. **116**, eds. R.M. Hjellming, D.M. Gibson, Reidel, Dordrecht, p. 139

Cassattella, A., Beeckmans, F., Benvenuti, P., Clavel, J., Heck, A., Lamers, H.J.G.L.M., Macchetto, F., Penston, M., Salvelli, P.L., Stickland, D.: 1979, *Astron. Astrophys.* **79**, 223

Castor, J.I., Lamers, H.J.G.L.M.: 1979, *Astrophys. J. Suppl.* **79**, 223

Drew, J.: 1985, *Monthly Notices Roy. Astron. Soc.* **217**, 867

Gabler, R., Gabler, A., Kudritzki, R.P., Puls, J., Pauldrach, A.W.A.: 1989, *Astron. Astrophys.* **226**, 162

van Gent, R.H., Lamers, H.J.G.L.M.: 1986, *Astron. Astrophys.* **158**, 335

Howarth, J.D., Prinja, R.K.: 1989, *Astrophys. J. suppl.* **69**, 527

Humphreys, R.M., Davidson, K.: 1979, *Astrophys. J.* **232**, 409

Humphreys, R.M., Davidson, K.: 1984, *Science* **223**, 243

Kudritzki, R.P., Pauldrach, A.W.A., Puls, J., Abbott, D.C.: 1989, *Astron. Astrophys.* **219**, 205 (Paper VI)

Kurucz, R.L.: 1979, *Astrophys. J. Suppl.* **40**, 1

Lamers, H.J.G.L.M., de Groot, M., Cassattella, A.: 1983, *Astron. Astrophys.* **128**, 299

Lamers, H.J.G.L.M., de Groot, M., Cassatella, A.: 1983a, *Astron. Astrophys.* **123**, L8

Lamers, H.J.G.L.M., Waters, L.B.F.M.: 1984, *Astron. Astrophys.* **136**, 37

Lamers, H.J.G.L.M., Korevaar, P., Cassattella, A.: 1985, *Astron. Astrophys.* **149**, 29

Lamers, H.J.G.L.M.: 1986, *Astron. Astrophys.* **159**, 90

Lamers, H.J.G.L.M.: 1986a, in *Luminous Stars in Associations and Galaxies*, eds. C.W.H. de Loore et al., Reidel, Dordrecht, p. 157

Lamers, H.J.G.L.M.: 1987, in *Instabilities in Luminous Early Type Stars*, eds. H.J.G.L.M. Lamers, C.W.H. de Loore, Reidel, Dordrecht, p. 99

Maeder, A.: 1983, *Astron. Astrophys.* **120**, 113

Maeder, A., Meynet, G.: 1987, *Astron. Astrophys.* **182**, 243 (MM)

© European Southern Observatory • Provided by the NASA Astrophysics Data System

1990A&A...237..409P

Markova, N., Kolka, I.: 1984, *Astrofiz.* **20**, 465
van den Oord, G.H.J., Waters, L.B.F.M., Lamers, H.J.G.L.M., Abbott, D.C., Bieging, J.H., Churchwell, E.: 1985, in "*Radio Stars*", *Astrophysics and Space Science Library*, Vol. **116**, eds. R.M. Hjellming, D.M. Gibson, Reidel, Dordrecht, p. 111
Panagia, N., Felli, M.: 1975, *Astron. Astrophys.* **39**, 1
Pauldrach, A.W.A., Puls, J., Kudritzki, R.P.: 1986, *Astron. Astrophys.* **164**, 86 (Paper I)
Pauldrach, A.W.A.: 1987, *Astron. Astrophys.* **183**, 295 (Paper III)
Pauldrach, A.W.A., Herrero, A.: 1988, *Astron. Astrophys.* **199**, 262
Pauldrach, A.W.A., Kudritzki, R.P., Puls, J., Butler, K.: 1990, *Astron. Astrophys.* **228**, 125 (Paper VII)
Pauldrach, A.W.A., Puls, J., Kudritzki, R.P.: 1989a, *Proc. IAU Colloquium No. 113* "*Physics of Luminous Blue Variables*", ed. K. Davidson, p. 261
Puls, J.: 1987, *Astron. Astrophys.* **184**, 227 (Paper IV)
Puls, J., Hummer, D.G.: 1987, *Astron. Astrophys.* **191**, 87
Puls, J., Pauldrach, A.W.A., Kudritzki, R.P.: 1989, *Proc. IAU Colloquium No. 113* "*Physics of Luminous Blue Variables*", ed. K. Davidson, p. 259
Stahl, O., Wolf, B., Zickgraf, F.-J.: 1987, *Astron. Astrophys.* **184**, 193
Waters, L.B.F.M., Lamers, H.J.G.L.M.: 1984, *Astron. Astrophys. Suppl.* **57**, 327
Waters, L.B.F.M., Wesselius, P.R.: 1986, *Astron. Astrophys.* **155**, 104
Wendker, H.J.: 1987, *Astron. Astrophys. Suppl.* **69**, 87
White, R.L., Becker, R.H.: 1982, *Astrophys. J.* **262**, 657
Wolf, B., Appenzeller, I., Stahl, O.: 1981, *Astron. Astrophys.* **103**, 94
Wolf, B., Stahl, O., de Groot, M.J.H., Sterken, C.: 1981, *Astron. Astrophys.* **99**, 351
Wright, A.E., Barlow, M.J.: 1975, *Monthly Notices Roy. Astron. Soc.* **170**, 41

© European Southern Observatory • Provided by the NASA Astrophysics Data System